HHS Public Access

Author manuscript

Dev Biol. Author manuscript; available in PMC 2025 February 01.

Published in final edited form as:

Dev Biol. 2024 February ; 506: 72–84. doi:10.1016/j.ydbio.2023.12.005.

Dgcr8 functions in the secondary heart field for outflow tract and right ventricle development in mammals

Silvia E Racedo[1], **Yang Liu**[4], **Lijie Shi**[1], **Deyou Zheng**[1,2,3], **Bernice E Morrow**[1,5,*]

[1]Department of Genetics, Albert Einstein College of Medicine, Bronx, NY, USA.

[2]Department of Neurology, Albert Einstein College of Medicine, Bronx, NY, USA.

[3]Department of Neuroscience, Albert Einstein College of Medicine, Bronx, NY, USA.

[4]Allergy, Pulmonary, and Critical Care Medicine, Vanderbilt University Medical Center, Bell Buckle, TN, USA.

[5]Departments of Pediatrics and Ob/Gyn & Population Health

Abstract

The *DGCR8* gene, encoding a critical miRNA processing protein, maps within the hemizygous region in patients with 22q11.2 deletion syndrome. Most patients have malformations of the cardiac outflow tract that is derived in part from the anterior second heart field (aSHF) mesoderm. To understand the function of *Dgcr8* in the aSHF, we inactivated it in mice using *Mef2c-AHF-Cre*. Inactivation resulted in a fully penetrant persistent truncus arteriosus and a hypoplastic right ventricle leading to lethality by E14.5. To understand the molecular mechanism for this phenotype, we performed gene expression profiling of the aSHF and the cardiac outflow tract with right ventricle in conditional null versus normal mouse littermates at stage E9.5 prior to morphology changes. We identified dysregulation of mRNA gene expression, of which some are relevant to cardiogenesis. Many pri-miRNA genes were strongly increased in expression in mutant embryos along with reduced expression of mature miRNA genes. We further examined the individual, mature miRNAs that were decreased in expression along with pri-miRNAs that were accumulated that could be direct effects due to loss of *Dgcr8*. Among these genes, were miR-1a, miR-133a, miR-134, miR143 and miR145a, which have known functions in heart development. These early mRNA and miRNA changes may in part, explain the first steps that lead to the resulting phenotype in *Dgcr8* aSHF conditional mutant embryos.

Graphical Abstract

*Corresponding author: bernice.morrow@einsteinmed.edu.

Conflict of interest

The authors declare no conflict of interest.

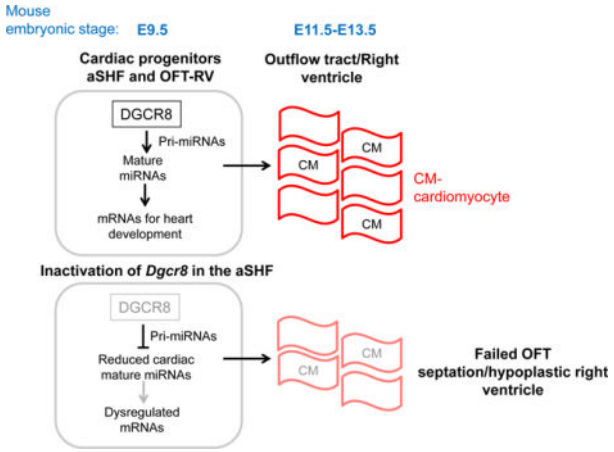

Author summary

The *DGCR8* gene encodes a subunit of a protein complex that processes miRNAs and it is in the hemizygously deleted region on chromosome 22 in patients with 22q11.2 deletion syndrome (22q11.2DS). To understand the specific functions of *Dgcr8* in mouse heart development, we inactivated it in the anterior second heart field. We found severe heart malformations, dysregulation of mRNA expression, increased expression of pri-miRNAs with decreased expression of mature miRNAs related to heart development. This work contributes to our understanding of *DGCR8* functions in heart development in mammals.

Introduction

The 22q11.2 deletion syndrome (22q11.2DS; Velo-cardio-facial syndrome, MIM# 192430; DiGeorge syndrome, MIM# 188400) is caused by a hemizygous 1.5–3 million base pair (Mb) deletion of chromosome 22q11.2. It occurs with a frequency of 1:1,000 fetuses and 1:4,000 live births (Botto et al. (2003); (McDonald-McGinn et al., 2015). There are different deletion sizes that occur in the region due to meiotic non-allelic homologous recombination between low copy repeats (LCR22; (Edelmann et al., 1999b). Most individuals have a 3 Mb deletion flanked by LCR22A-D (Edelmann et al., 1999a; Edelmann et al., 1999b; Shaikh et al., 2000). There are 46 known protein coding genes within the most frequent sized, 3 Mb interval (Cleynen et al., 2021). There are 30 known protein coding genes in the nested proximal, 1.5 Mb region and this deletion is flanked by low copy repeats, LCR22A-B (Cleynen et al., 2021; Edelmann et al., 1999b; McDonald-McGinn et al., 2015; Shaikh et al., 2000). Although most affected individuals have a 3 Mb deletion, those with the 1.5 Mb deletion have similar phenotypes, implicating the nested, 1.5 Mb region as containing critical genes for the syndrome (Edelmann et al., 1999a; Shaikh et al., 2000). Approximately 60–70% of affected 22q11.2DS individuals have congenital heart disease (CHD) due to malformations of the cardiac outflow tract (OFT) and/or aortic arch, frequently referred to as conotruncal defects (Goldmuntz, 2020; Unolt et al., 2018). Most typical anomalies include tetralogy of Fallot, interrupted aortic arch type B, or right sided aortic arch with an aberrant left subclavian artery (Goldmuntz, 2020; Unolt et al., 2018). These defects arise from progenitor cells in the pharyngeal apparatus of the early mammalian embryo.

The pharyngeal apparatus is a temporary embryological structure lateral to the head, composed of cells of all three germ layers including the mesoderm. The heart and aortic arch forms in significant part, from two fields of mesodermal cells, referred to as the first heart field (FHF) and the second heart field (SHF). They are named as such according to the position of the cells with respect to each other in the embryo and order of migration from the common progenitor cells of both lineages (Kelly, 2012, 2023; Kelly et al., 2014). FHF and SHF cells differentiate to cardiomyocytes and contribute to distinct regions of the heart during later development (Buckingham et al., 2005). The SHF itself, can be further subdivided to the anterior SHF (aSHF) forming the cardiac OFT and right ventricle (RV) as well as the posterior SHF forming the inflow tract, respectively, based upon rostral-caudal position, gene expression and cell lineage tracing studies (Kelly, 2023; Watanabe et al., 2010; Xie et al., 2012; Zhou et al., 2017). One of the key functions of aSHF cells is to maintain a progenitor cell state while allowing expansion of the RV with OFT and differentiation in a time-controlled manner (Ai et al., 2007; Rana et al., 2014). The aSHF is considered a critical population in association with conotruncal heart defects in patients with 22q11.2DS (Racedo et al., 2017). The aSHF is marked by the *Mef2c-AHF-Cre* lineage and the expression of the transcription factor gene, *Tbx1*, while the pSHF, caudally located, is marked by expression of *Tbx5* (De Bono et al., 2018). There are other mesodermal cell types that contribute to the heart including the proepicardial organ that gives rise to the epicardium, referred to as the juxta-cardiac field (Tyser et al., 2021). Neural crest cells are another population of cells that migrate from the closing neural tube to the cardiac OFT to form the septation between the aorta and pulmonary trunk (Kirby, 1993). The pharyngeal arches within the pharyngeal apparatus form in a rostral to caudal manner during embryogenesis. The pharyngeal arch arteries are present within each arch and contain an endothelium derived from the aSHF and smooth muscle derived from neural crest derived cells, which become remodeled to form the aortic arch and arterial branches (Wang et al., 2017; Warkala et al., 2021).

The *DGCR8* gene is one of 30 known coding genes in the nested 1.5 Mb region between LCR22A-B. It is therefore hemizygously deleted in the great majority of patients with 22q11.2DS. This gene encodes a double-stranded RNA-binding protein that is an essential component of the DGCR8/DROSHA nuclear complex that processes primary-miRNA (pri-miRNA) genes into pre-miRNAs. DGCR8 as part of the miRNA processor complex, binds RNA non-specifically that is needed for processing pri-miRNAs (Roth et al., 2013). In mammals, *Dgcr8* is ubiquitously expressed in all cells. To study its role in various cell lineages in heart development, different *Cre* mouse lines have been used for tissue specific inactivation of *Dgcr8*. Inactivation of *Dgcr8* in early mesoderm progenitor cells using $Mesp1^{Cre}$, affecting the FHF and SHF, resulted in early lethality at E10.5-E11.5 with severe dilation of the heart and abnormal cardiomyocytes (Chen et al., 2019). Inactivation in vascular smooth muscle resulted in lethality at E12.5-E13.5 with severe overall malformations in the embryos (Chen et al., 2012). *Dgcr8* was inactivated in neural crest cells using *Wnt1-Cre* and this resulted in perinatal lethality (Chapnik et al., 2012). Resulting conditional null embryos had defects that included persistent truncus arteriosus with a ventricular septal defect and aortic arch artery anomalies, due to apoptosis of progenitor neural crest cells (Chapnik et al., 2012).

Many miRNAs together regulate biological processes in the cell by inhibiting expression of a broad range of mRNA mediated proteins, thereby acting as switches in cellular development or homeostasis. We are interested in determining the role of *Dgcr8* in the aSHF mesoderm for cardiac development, because this is the main population affected in patients with 22q11.2DS. We used *Mef2c-AHF-Cre* mice (Verzi et al., 2005) and crossed them with *Dgcr8* floxed mice (Rao et al., 2009). In this report, we found that *Dgcr8* conditional null mutant embryos died by E14.5 with hypoplasia of all aSHF derivatives as well as the left ventricle. We present results of gene expression profiling of mRNAs, pri-miRNAs and miRNAs in *Dgcr8* mutant embryos versus controls at E9.5, which is the stage when the aSHF cells migrate to the OFT prior to observed malformations.

Methods

Mouse mutant alleles

The following mouse mutant alleles used in this study have been previously described: $Dgcr8^{f/+}$ (flox = f; MMRRC #32051; (Rao et al., 2009)), *Mef2c-AHF-Cre/+* (Verzi et al., 2005), $ROSA26\text{-}GFP^{f/+}$ (RCE:loxP)(Sousa et al., 2009). To generate *Mef2c-AHF-Cre/+;*$Dgcr8^{f/f}$ mutant embryos, *Mef2c-AHF-Cre/+* transgenic male mice were crossed to $Dgcr8^{f/f}$ mice to obtain male *Mef2c-AHF-Cre/+;*$Dgcr8^{f/+}$ mice that were then crossed with female $Dgcr8^{f/f}$ with $ROSA26\text{-}GFP^{f/f}$ mice to obtain embryos that are *Mef2c-AHF-Cre/+;*$Dgcr8^{f/f}$*;ROSA26-*$GFP^{f/+}$ or *Mef2c-AHF-Cre/+;*$Dgcr8^{f/+}$*;ROSA26-*$GFP^{f/+}$ carrying the GFP fluorescent reporter. The $Dgcr8^{f/f}$ line used for the experimental crosses have been maintained in a mixed C57Bl/6;Swiss Webster background. The reporter $ROSA26\text{-}GFP^{f/+}$ allele was added to the $Dgcr8^{f/f}$ line when visualizing *Mef2c-AHF-Cre* lineage. The PCR strategies for mouse genotyping have been described in the original reports and are available upon request.

Ethics statement

All experiments including mice were carried out according to regulatory standards defined by the NIH and the Institute for Animal Studies, Albert Einstein College of Medicine (https://www.einstein.yu.edu/administration/animal-studies/), Institutional Animal Care and Use Committee, protocol # 00001034.

Mouse embryo heart histology and phenotypic analysis

Mouse embryos were isolated in phosphate-buffered saline (PBS) and fixed in 10% neutral buffered formalin (Sigma Corp.) overnight. Following fixation, the embryos were dehydrated through a graded ethanol series, embedded in paraffin and sectioned at 5 μm (micrometers). All histological sections were stained with hematoxylin and eosin using standard protocols. Staining was performed in the Einstein Histopathology Core Facility (http://www.einstein.yu.edu/histopathology/page.aspx). The histological sections were analyzed morphologically using light microscopy.

Proliferation analysis on tissue sections

After fixation for 2 hours with 4% PFA in PBS at 4°C, paraffin sections were obtained at a thickness of 10 μm and then they were permeabilized in 0.5% Triton X-100 for 5 min.

Blocking was performed with 5% serum (goat or donkey) in PBS/0.1% Triton X-100 (PBT) for 1 hour. Primary antibody was diluted in blocking solution (1:500) and incubated for 1 hour. Proliferation of cells was assessed by immunofluorescence using anti-phospho Histone H3 (Ser10; 06–570 Millipore). Sections were washed in PBT and incubated with Alexa Fluor 568 goat a-rabbit IgG (A11011 Invitrogen; 1:500) for 1 hour. Slides were mounted in hard-set mounting medium with DAPI (Vector Labs H-1500). Images were captured using a Zeiss Axio Observer microscope. To perform statistical analysis of cell proliferation, we first counted the GFP positive cells from the *Mef2c-AHF-Cre* lineage in tissue sections of the caudal pharyngeal apparatus in embryos, consisting of pharyngeal arches 2–4, located dorsal to the heart, and then calculated the average cell counts per tissue section for each embryo. Then we counted all proliferating cells in each section and calculated the ratio of proliferating cells within the *Mef2c-AHF-Cre* lineage. The mean and standard error of the average cell counts for controls and *Dgcr8* conditional null mutant embryos was determined, and they were compared using the Student's t-test. Natural GFP from the reporter or an antibody for GFP (Abcam #6290) was used to distinguish the aSHF cells. The aSHF from at least four embryos per genotype from at least three independent litters were used in each assay.

Direct fluorescence to trace the *Mef2c-AHF-Cre* lineage

Images were generated from GFP expressing embryos by direct fluorescence immediately following dissection. For tissue sections, embryos were fixed for 2 hours at stage ≤ E10.5 (30 – 32 somite pairs). Fixation was carried out in 4% PFA in PBS at 4°C. After fixation, the tissue was washed in PBS and then cryoprotected in 30% sucrose in PBS overnight at 4°C. Embryos were embedded in OCT and cryosectioned at 10 μm. Images were then captured using a Zeiss Axio Observer microscope.

Gene expression profiling on microarrays

Embryos at E9.5 (19 – 21 somite pairs) were used for global gene expression studies. To obtain enough RNA for microarray hybridization experiments, microdissected aSHF (pharyngeal arches 2–4; excluding the heart) of *Dgcr8* conditional null and controls (*Dgcr8*$^{f/+}$; without *Mef2c-AHF-Cre*) were pooled, separately, in four pools, each of groups of four or six embryos according to the genotype for a total of 27 embryos. The same was done for the microdissected OFT with RV (OFT-RV). We then purified mRNA using the miRNeasy Qiagen method as per manufacturer's instructions. Four separate pools of each genotype of five embryos each were generated and processed. The tissue was homogenized in Buffer RLT (QIAGEN). Total RNA was isolated with the RNeasy Micro Kit according to the manufacturer's instructions. Quality and quantity of total RNA were determined using an Agilent 2100 Bioanalyzer (Agilent) and an ND-1000 Spectrophotometer (NanoDrop), respectively. Biotinylated single-stranded cDNA targets were amplified from 100 nanograms (ng) starting total RNA using the Ovation RNA Amplification System V2 and FLOvation cDNA Biotin Module V2 (NuGEN). A total of 3.75 mg of cDNA was hybridized to the GeneChip Test3 array (Affymetrix) to test the quality of the labeled target. Nucleic acid samples that passed quality control were then hybridized to the microarrays. The resulting cDNA was applied to Affymetrix Mouse GeneST 1.0 microarrays and separately miRNAs were processed on Affymetrix miRNA 4.0 microarrays in the Genomics Core at Albert

Einstein College of Medicine. The microarrays were performed per genotype in two to three separate batches. Hybridization, washing, staining and scanning were performed in the Genomics Core at Albert Einstein College of Medicine according to the Affymetrix manual.

Microarray data analysis

Affymetrix data analysis was performed using standard R statistical packages. Briefly, GeneChip data were pre-processed by the 'oligo' package (Carvalho and Irizarry, 2010), which implements the Robust Multichip Average (RMA) algorithm with background correction, quantile normalization and gene level summarization (Irizarry et al., 2003). Afterwards, for convenience of comparison, only probe-sets assigned to genes were kept for subsequent analysis. Multiple probe-sets for the same gene were collapsed by "average" to obtain a single measurement per gene (Miller et al., 2011). We applied ComBat, an efficient batch effect removal approach, to remove batch effects by using the R package "sva" (v3.38.0) (Johnson et al., 2007). This analysis detected some individual microarrays of poor quality that were then excluded. To keep a balance between controls and mutants, we analyzed three microarrays per genotype. The 'Limma' package (v3.46.0) was used for determining differential expression (Ritchie et al., 2015). To adjust for experimental or technical batch effects (Nygaard et al., 2016), we used Limma by adding the algorithm 'blocking for batch' in the model. Genes with individual p-values < 0.05 were further explored. The microarray data has been deposited to the GEO database (accession number: GSE186064).

Quantitative RT-PCR

Embryos at E9.5 (19 – 21 somite pairs) and E11.5 were used for quantitative gene expression studies of the microdissected aSHF or the OFT-RV, from each *Dgcr8* conditional null and control (*Dgcr8*$^{f/+}$) embryo that were pooled in groups according to genotype. To obtain enough total RNA and minimize variability of gene expression in individual embryos, each biological replicate was from six embryos of the same genotype at E9.5 from at least three independent litters. Three biological replicates were performed per genotype. The tissue was immediately frozen, samples were homogenized and total RNA was isolated with the RNeasy Micro Kit (Qiagen). Quality and quantity of total RNA was determined using an Agilent 2100 Bioanalyzer (Agilent) and a ND-1000 Spectrophotometer (NanoDrop), respectively. Single-stranded cDNA targets were amplified from 100 nanograms (ng) starting total RNA using the Ovation RNA Amplification System V2 and FL- Ovation cDNA Biotin Module V2 (NuGEN). The mRNA levels were measured using TaqMan Gene Expression assays (Applied Biosystems) for each gene and were carried out in triplicate using *18S* (RNA, 18S ribosomal 1), *Actb* (Actin, beta) and *B2m* (Beta-2-microglobulin) genes as normalization controls. TaqMan probes and primer sets were obtained from the Applied Biosystems Gene Expression Assay database (http://allgenes.com). Probes are provided in Supplementary Table 1. Samples were processed in standard 96-well plates (20 μl final volume per reaction and each reaction in triplicate containing 25 ng of cDNA) on an ABI 7900HT Q-PCR apparatus. The SDS 2.2 software platform (Applied Biosystems) was used for the computer interface with the ABI 7900HT PCR System to generate normalized data, compare samples, and calculate relative quantity. Statistical significance

of the difference in gene expression was estimated using ANOVA and the two-tailed t-test independently when the type of comparison allowed for it.

Web resources

http://www.omim.org

http://genome.ucsc.edu/

http://www.R-project.org

https://string-db.org

https://digitalinsights.qiagen.com

Results

Persistent truncus arteriosus and hypoplastic ventricles in *Dgcr8 conditional null* mutant embryos

To determine a specific role of *Dgcr8* in the aSHF, we inactivated one or both floxed alleles of *Dgcr8* in the *Mef2c-AHF-Cre* domain to generate conditional heterozygous (*Mef2c-AHF-Cre;Dgcr8*$^{f/+}$) and conditional null (*Mef2c-AHF-Cre/+;Dgcr8*$^{f/f}$) mutant embryos as shown in Figure 1. We refer to conditional null embryos as *Dgcr8* cKO mutants. We evaluated histological sections from *Dgcr8* conditional heterozygous embryos and compared them to *Dgcr8* cKO embryos at E13.5 (Figure 1A–B). This is the embryonic stage just before the conditional null mutant embryos died, at E14.5. Heterozygous embryos had normal hearts and survived normally after birth and are considered as controls herein (Figure 1). The *Dgcr8* cKO embryos had a fully penetrant persistent truncus arteriosus (PTA), atrioventricular valve malformations, hypoplastic ventricles with thin ventricular walls and immature trabeculae as well as a ventricular septal defect (VSD; Figures 1A–C). The *Dgcr8* conditional heterozygous and *Dgcr8* cKO embryos included a *ROSA26-GFP* reporter to trace the aSHF lineage. Lineage tracing revealed no gross differences in the population of GFP expressing derivative OFT and RV cells from the aSHF in *Dgcr8* cKO embryos as compared to controls (Figure 1D). This suggests that the left ventricular and atrioventricular valve malformations are likely secondary to the aSHF defects since the lineage does not encompass these regions, supporting the possibility of hemodynamic alterations at this developmental stage.

To understand when defects first became apparent, we examined *Dgcr8* control and *Dgcr8* cKO embryos at earlier embryonic stages. There were no noticeable defects in the pharyngeal apparatus, OFT and ventricle in conditional heterozygous and *Dgcr8 c*KO embryos by histological analysis at E10.5 (Figure 2A and 2B). In addition to the aSHF mesoderm, cardiac neural crest cells are present in the caudal pharyngeal apparatus (Erhardt et al., 2021). There were no obvious defects observed within this part of the embryo. The septum between the RV and LV begins to form at E11.5. Neural crest cells fill the distal cardiac cushions of the OFT, while endocardial derived mesenchyme cells fill most of the proximal OFT. There was not an obvious reduction in the neural crest cell population at

E11.5 (Supplementary Figure 1). At E11.5, *Dgcr8* cKO embryos had visible defects that included misalignment of the OFT cushions (Figure 2A; 2C, left) and RV defects including an irregular morphology with smaller relative size compared to the left ventricle, and a thinner RV myocardial wall (Figure 2A; Figure 2C, right). At E12.5, all control embryos had a septum between the aorta and pulmonary trunk as well as an intact ventricular septum, while all *Dgcr8* cKO embryos had a PTA with a VSD and a hypoplastic RV (Figure 2A and 2D).

Proliferation and apoptosis assays in *Dgcr8 LOF* embryos

We then wondered whether there were defects in cell proliferation at E10.5 prior to observing phenotypic abnormalities at E11.5. Proliferation assays of the GFP expressing aSHF lineage cells (Figure 3A) did not show significant differences in the mitotic indexes between controls and *Dgcr8* cKO embryos at E10.5 (n = 7 for both genotypes; Figure 3B). The total number of GFP expressing cells in the OFT in *Dgcr8* cKO embryos versus controls were similar and were not significantly different as determined using Student's t-test, suggesting that cell migration to the OFT was not affected at E10.5 (n=7 for both genotypes; Figure 3C).

Gene expression analysis of the aSHF in *Dgcr8* cKO embryos at E9.5

To determine how loss of *Dgcr8* could result in aSHF derived malformations, we performed gene expression profiling at E9.5, prior to when defects were first observed. We isolated the aSHF in the pharyngeal apparatus, dorsal to the heart, and separately, the OFT with the RV at stage E9.5 (19 – 21 somite pairs; Supplementary Figure 2) and performed Affymetrix microarray analysis. We performed four biological replicates of control and *Dgcr8* cKO tissues.

We found 338 coding mRNA genes were altered in expression in the aSHF of which 174 were up-regulated and 164 down-regulated, with mild but reproducible fold changes observed (individual $p<0.05$; Supplementary Table 2). Representative and biologically relevant genes are shown in the heatmap in Figure 4A. We examined gene ontology (GO) categories of the upregulated genes in the aSHF using ToppGene software (http://toppgene.cchmc.org). There was borderline significance of the gene ontology category "chemorepellent activity" (GO:0045499; Bonferroni P value 2.37×10^{-2}, Supplementary Table 3). Of the GO categories among all genes decreased in expression, there was only one nominally significant GO molecular function category that was "neurotrophin binding" (GO: 0043121; Bonferroni P value 4.68×10^{-2}). We then examined the function of the top 50 genes with greatest fold change using STRING software (Supplementary Table 2). We selected transcription factors and signaling molecules for further examination (colored dots in Figure 4A). Among the top 50 downregulated genes included, *Barx1, Tbx18, T, Twist2, Epha3, Foxf2, Hoxb4* and *Foxa2*. Among the top 50 genes that were increased in expression were *Cited4, Fgf8, Meox1, Sp5* and *Fgf4*. Some of these genes that were altered are shown in a volcano plot (Figure 4B). We validated expression of a subset of genes that were decreased or increased in expression by quantitative RT-PCR (qRT-PCR; raw data is provided in Supplementary Table 4) based upon STRING analysis, and we found trends consistent with microarray results (Figure 4C). Only some were significantly changed

among the total, and we suggest the reason is that the tissue size that was used for RNA isolation was very tiny. We performed GO analysis of the genes selected for qRT-PCR for the aSHF based upon STRING analysis, and the top GO category decreased was genes relevant for embryonic morphogenesis, while the top GO category increased was genes for skeletal system development (Figure 4D). Most of these are transcription factors are involved in morphogenesis of the pharyngeal apparatus. This suggests at this developmental stage, loss of *Dgcr8* results in dysregulated expression of genes that are needed for morphogenesis. We used Ingenuity Pathway Analysis software of all the genes altered in expression, to identify downstream canonical pathways that were affected. We identified two overlapping pathways from genes that were decreased in expression. One was Integrin signaling pathway (Bonferroni P value 2.42 × 10–3, *Cav1, Itga4, Pak3, Pfn4, Rhob, Rock1*) and the other was the Ephrin receptor signaling pathway (Bonferroni P value 9.59 × 10–3, *Epha3, Itga4, Pak3, Pdgfc, Rock1*). Alteration of these pathways could affect progenitor cells in the aSHF and neural crest cells in the cardiac outflow tract needed for septation. We did not identify a significant pathway affected by genes that were increased in expression. Expression of *Dgcr8* was slightly reduced in the aSHF at this stage by microarray analysis (135 from the top of fold change; Supplementary Table 2) and was not changed by qRT-PCR (Supplementary Table 4). This could be due to lack of sensitivity of bulk tissue microarray analysis with only a subset of cells derive from the *Mef2c-AHF-Cre* lineage. Consistent with some reduction of *Dgcr8* expression, we found a very robust increase of expression of pri-miRNAs in the aSHF tissue (Figure 4B, which will be presented more below). We next examined mRNA genes altered in the OFT-RV in *Dgcr8* cKO embryos.

Disruption of cardiomyocyte developmental genes in the OFT-RV in *Dgcr8* cKO embryos at E9.5

Next, we examined mRNA expression changes in the OFT-RV at E9.5 in *Dgcr8* cKO versus control embryos. A total of 916 mRNAs were altered in expression including 546 that were decreased and 370 that were increased in expression (individual P value <0.05; Supplementary Table 5). As for the aSHF, alteration of mRNA expression was modest and representative genes increased and decreased are indicated in the heatmap in Figure 5A. The top GO category for molecular function overall in genes decreased, was “ion channel activity” (GO:0005216; Bonferroni P value 3.3×10^{-2}) and the top biological process was “actin filament-based process” (GO:0030029; Bonferroni P value 4.29×10^{-4}) and “cardiac conduction” (GO:0061337; Bonferroni P value 4.10×10^{-3}; Supplementary Table 6). One of the top biological processes was “heart development (GO:0007507; Bonferroni P value 2.95×10^{-2}). This top biological process of genes decreased in expression included genes such as *Erbb3, Pdgfa, Twist1, Pln, Angpt1, Snai1, Apln* and *Nfatc4*. These genes are relevant to cardiac valve formation and cardiomyocyte differentiation. GO analysis identified genes for protein kinase activity as significantly increased and included ‘transferase activity, transferring phosphorous-containing groups’ (GO:0016772; Bonferroni P, 1.55×10^{-4}; Supplementary Table 7). A volcano plot was generated that highlighted the changes of some of the genes that were identified (Figure 5B).

As for the aSHF, we next used STRING software to examine top 50 genes with greatest fold change in expression in mutant embryos. We focused upon genes encoding transcription

factors and signaling molecules (Supplementary Table 5). Among the top 50 genes that were reduced in expression, included *Pdgfc, Dgcr8, Twist1, Nr2f2, Erbb3, Smad9, Cldn5* and *Ncam1*. Among the top 50 genes increased in expression, there were no obvious genes identified encoding transcription factors or signaling molecules. We validated expression of a subset of genes both increased and decreased in expression by quantitative RT-PCR at E9.5 and E11.5 (Figure 5C and D; raw data is provided in Supplementary Tables 8 and 9). As for the aSHF, we found trends of gene expression changes of genes for cardiac differentiation were consistent between qRT-PCR and microarray experiments, with some changes being statistically significant at E9.5 (Figure 5C). The top GO category of selected genes that were validated was Heart Development and Positive Regulation of Developmental Process, for those decreased and increased in expression, respectively (Figure 5E). When taken together, the data suggests that genes important for heart development are disrupted by loss of *Dgcr8* in the OFT-RV, some of which derive from the aSHF in the pharyngeal apparatus at earlier time points.

Expression of *Dgcr8* was reduced as can be observed from the mRNA microarray analysis (Supplementary Table 5) and by qRT-PCR (Supplementary Table 8). As for the aSHF, at E9.5, we found that the pri-miRNAs showed robust increase in expression (Figure 5B). In contrast to the aSHF, where there is a mixture of mesoderm and cardiac neural crest cell types, the OFT-RV consists of fewer cardiac neural crest cells because they have not yet migrated into the OFT. Thus, changes in gene expression did not include alteration in neural crest cells. At E11.5, the cardiac signaling and differentiation genes were all decreased in expression (Figure 5D; Supplementary Table 9). The decrease in specific gene expression at E11.5 might be secondary to morphological defects that were already present at this time point. Also, changes at this stage could include additional cell types such as neural crest derived cells.

Pri-miRNA expression analysis

We next examined pri-miRNA expression changes from the mRNA microarray for the aSHF (Supplementary Table 10) and OFT-RV (Supplementary Table 11). The expression of pri-miRNA genes is regulated similarly to mRNA genes (Wang et al., 2007). Therefore, where and when in development that a pri-miRNA is expressed, DGCR8 should process the precursors to mature miRNAs (Isakova et al., 2020). From the literature, pri-miRNAs show a broader expression pattern than mature miRNAs but most show some specificity (Lee et al., 2008). Further, there is a DGCR8-responsive RNA element on certain pri-miRNA genes that may make it more efficient in processing (Nogami et al., 2021). We found 84 pri-miRNA genes were increased in expression in *Dgcr8* cKO and one was decreased (Supplementary Table 10). A total of 169 were increased in the OFT-RV and 36 were decreased in expression in *Dgcr8* cKO embryos (Supplementary Table 11). There are a total of 1,234 pri-miRNA genes that are listed in the miRbase database (miRbase.org), suggesting that not all were expressed or expression was not detected by our method. Some were also decreased in expression, suggesting possible indirect mechanisms.

A total of 80 pri-miRNA genes that were increased in expression were shared between the aSHF and the OFT-RV, with only four pri-miRNA genes found exclusively in the aSHF,

while 112 were exclusively found increased in the OFT-RV (Figure 6A; Supplementary Table 12). It is possible that these genes are normally enriched in expression in these cells in the embryo and that inactivation of *Dgcr8* affected those that would normally be expressed. As expected, GO analysis identified mRNA base-pairing post-transcriptional repressor activity (GO: 1903231; corrected P value, 1.04×10^{-132}) as the top most significant category (Supplementary Tables 13 and 14). Of note, several among the top 50 GO categories included vascular development categories (e.g. GO:1901343; corrected P value, 1.11×10^{-24}; Supplementary Tables 13 and 14). This indicates that altered expression could be relevant to the primary defects observed at slightly later developmental stages.

Mature miRNA expression profiling

We next performed mature miRNA gene expression profiling using miRNA specific microarrays to examine the miRNA changes in the aSHF and OFT-RV. We found, 175 and 243 mature miRNAs were significantly changed in the aSHF and OFT-RV, respectively (P value<0.05; Supplementary Tables 15 and 16). We expected to observe a decrease in expression of miRNAs. For the aSHF, we found a total of 50 were increased in expression and 125 were decreased (Supplementary Table 15). For the OFT/RV, a total of 105 were increased and 138 were decreased. Surprisingly, almost half were increased in expression in both tissues. This suggests perhaps secondary changes in miRNA gene expression.

Since many pri-miRNA genes were increased in expression, possibly due to lack of processing to miRNAs by loss of *Dgcr8*, we compared the pri-miRNAs that were increased in expression to expression changes in miRNA genes. The reason is that some of these changes might be correlated. We found that increased expression of pri-miRNA genes was partially correlated with decreased expression of mature miRNAs (Supplementary Table 17). The focus then turned to examine the subset of pri-miRNA genes that were increased in expression and the corresponding mature miRNAs that were decreased in expression, because they may be a primary result of failed processing of pri-miRNAs. These genes were examined in the aSHF and OFT-RV and a summary of the results is shown in Figure 6B. Despite a great overlap in the pri-miRNA genes between the aSHF to the OFT-RV (Figure 6A), only half the mature miRNAs overlapped between both tissues (Figure 6B). This could be due to multiple steps of regulation of miRNA processing that are not yet fully understood. A total of 13 miRNAs overlapped in both tissues (Figure 6B). A total of 12 mature miRNA genes were uniquely decreased in expression in the aSHF (Figure 6B). A total of 27 mature miRNAs were uniquely decreased in the OFT-RV (Figure 6B).

We then examined the known expression or function of mature miRNAs for heart development as reviewed by Zare and colleagues (Zare et al., 2023) and elsewhere in the literature (Supplementary Table 17). From this, we indicated which genes that are functionally relevant to heart development as shown in red color font in Figure 6B. We show the Log2 fold change of a subset of pri-miRNA genes that were increased in expression (gray color) with respect to the mature miRNA genes that were decreased (aqua color) from Supplementary Tables 15 and 16, and indicated which ones are related to heart development (Figure 6C). In a previous study, *Dgcr8* was inactivated throughout the early embryonic mesoderm using the $Mesp1^{Cre}$ allele (Chen et al., 2019). As expected, because *Mesp1* is

expressed earlier and marks more cells, the cardiac phenotype was more severe in *Mesp1* cKO versus *Mef2c-AHF-Cre* cKO embryos (Saga et al., 1999). The *Mesp1* cKO embryos died between E9.5–11.5 with severe dilation of the heart, heart looping and cardiomyocyte defects (Chen et al., 2019). Nonetheless, many of the top miRNA genes reduced in expression in the *Mesp1*^{Cre} study by Chen and colleagues (Chen et al., 2019) were found in our analysis (Fig. 6B and C). The top miRNA genes that were reduced in expression in the hearts in the Zare et al. study was linked to mRNAs involved in angiogenesis and blood vessel morphogenesis (Zare et al., 2023). This included miR-541, that was shown functionally to mediate some of the defects that occurred by inactivation of *Dgcr8* (Chen et al., 2019). In our study, we found that pri-miR-541 was slightly increased and miR-541 was slightly decreased in expression in the aSHF but not changed in the OFT-RV at E9.5 (Fig. 6C). Thus, it is possible that the phenotype we observed in our *Dgcr8* conditional mutant embryos using *Mef2c-AHF-Cre* involves some but not all the miRNAs found in the previous study using *Mesp1*^{Cre}.

There were greater fold changes of pri-miRNA genes increased in expression with decreased mature miRNA expression in the OFT-RV as compared to the aSHF (Fig. 6A–B). When taken together with the larger number of miRNA genes affected, the greatest changes were in the OFT-RV, which is the target tissue affected in the *Dgcr8* cKO embryos. We suggest that disruption of the miRNA genes that are relevant to heart development might contribute to the observed phenotype in the mutant embryos.

There are many predicted mRNA target genes regulated by miRNAs and vice versa. One goal would be to test whether the mRNAs that were increased in expression would be targets of the miRNAs that were decreased in expression. This involves examining miRNA target genes, and usage of target prediction software. One of the disadvantages of usage of target predication software is that few have been experimentally validated. For our strategy, we used three web-based predication tools, TargetScan (Lewis et al., 2005), Dianatools (Doench and Sharp, 2004) and miRanda (John et al., 2004). We considered a target mRNA if the miRNA-mRNA prediction was identified in all three tools, thus optimizing the robustness of the analysis. As shown in Supplementary Figure 3, some of the mRNAs are miRNA target genes. We found that 14% of the differentially expressed mRNAs between aSHF and OFT-RV in *Dgcr8* cKO embryos were potential miRNA targets (Supplementary Figure 3).

Discussion

In this report, we inactivated *Dgcr8* in the aSHF using the *Mef2c-AHF-Cre* allele to understand its role in the formation of the cardiac OFT and RV. We found that *Dgcr8* conditional mutant embryos had a hypoplastic OFT and RV at E11.5–12.5. This then affected heart development such that all conditional null embryos died by E14.5 with a PTA and hypoplastic ventricles. To understand the molecular basis of the defects, mRNA and miRNA gene expression profiling was performed at E9.5, before morphology defects were observed. We found altered expression of mRNA genes relevant to development of the heart. The greatest fold change during early development was an increase in expression of pri-miRNA genes, of which a subset correlated with reduced mature miRNAs. Most of the mature miRNAs are relevant to cardiac development, in particular in the OFT-RV. There is

a complex relationship between the mRNA gene expression changes and miRNAs, along with the pathogenesis of the defects in the aSHF conditional mutant embryos. We therefore investigated the literature to help understand the genes altered in expression (mRNA and miRNA) downstream of *Dgcr8* gene inactivation.

In a previous study, *Dgcr8* was inactivated throughout the early embryonic mesoderm using the *Mesp1*^{Cre} allele as described by Zare et al. (Zare et al., 2023). The cardiac phenotype was more severe in *Mesp1* cKO versus our *Mef2c-AHF-Cre* cKO embryos. This is because *Mesp1* is expressed earlier and more widely and the lineage includes a broader region than for *Mef2c-AHF-Cre* (Zare et al., 2023). The *Mesp1* cKO embryos died between E9.5–11.5 with severe dilation of the heart, heart looping and cardiomyocyte defects (Zare et al., 2023). Bulk transcriptomic analysis of hearts was performed at E9.5, and they found 857 genes were upregulated and 1,080 were downregulated in which genes involved in angiogenesis (e.g. *Pecam1*, *Ctgf*, *Sox17*), metabolic process and apoptosis were upregulated. Genes involved in RNA splicing, cell cycle and heart development were downregulated, (e.g. *Gata4*, *Tnni3*, *Tbx5*).

The *Mef2c-AHF-Cre* lineage represents a small subset of the total *Mesp1* lineage. One of the main GO categories of mRNAs decreased in expression for the OFT-RV was those involved in cardiac development. However, there were also other GO categories of genes involved in ion channel activity and cardiac conduction, which might suggest that besides developmental genes that loss of *Dgcr8* affected cardiac muscle function. We examined miRNA target gene prediction software to understand how loss of *Dgcr8* could affect expression of specific mRNAs. This software predicts thousands targets but most are not experimentally validated. In our analysis we found approximately 14% of the mRNAs were targets of miRNAs. Nonetheless, the pri-miRNA and miRNA pairs that we identified are shared with miRNAs with the greatest fold decrease in the Zare et al study of heart development, suggesting a subset of the mechanisms are shared in cardiogenesis. We also examined the biological functions of some of the miRNA genes that have been studied experimentally.

Among the miRNA genes that were reduced in expression in our study were, miR-1 and MiR-133a. These genes are known to function in cardiac development (Cordes and Srivastava, 2009). These two miRNA genes were also decreased in expression in the recent study in which *Dgcr8* was inactivated using *Mesp1*^{Cre} (Chen et al., 2019). The two miRNA's, miR-1 and miR-133, are implicated to play a key role in cardiomyocytes in heart development (Cordes and Srivastava, 2009). These two genes derive from a common precursor, and this precursor transcript is a result of a gene duplication, mapping to mouse chromosome 18 and 2, respectively. The mature miRNAs from the different loci are identical in sequence and show similar expression patterns (Wystub et al., 2013). In the aSHF, we found more modest changes in expression compared to that of the OFT-RV. These two genes are co-expressed in the heart but less so in the pharyngeal arches. *Hand2*, encoding a basic-helix-loop-helix transcription factor, that is required for cardiogenesis is regulated by miR-1 (Zhao et al., 2005) and miR-133 (Vo et al., 2010). Inactivation of miR-1–2 (Zhao et al., 2007) or inactivation of both miR-133a-1 and miR-133a2 (Liu et al., 2008) resulted in a ventricular septal defect. The hearts of miR-133a-1 and miR-133a2 knockout embryos

had enlarged hearts with thinner myocardial walls and dilated right ventricular chamber with dysregulation of the cell cycle (Liu et al., 2008). We did not observe a change in *Hand2* expression at E9.5 in *Dgcr8* cKO embryos. Perhaps a lack of alteration of *Hand2* expression in *Dgcr8* cKO embryos, is a result of the later and narrower expression domain of *Cre* using the *Mef2c-AHF-Cre* allele that was used in our study, or that we did not examine later stages.

Two other miRNA genes that we identified in our study are of particular interest for heart development. The miRNA genes for miR-143 and miR145 are encoded for by the same precursor and are expressed in the aSHF, OFT and the rest of the heart (Cordes et al., 2009). We found that the expression of the precursor was increased and expression of miR-143 was decreased in the aSHF and miR-145 were decreased in the aSHF and OFT-RV in *Dgcr8* cKO embryos. These miRs were also decreased in expression when *Dgcr8* was inactivated using $Mesp1^{Cre}$ (Chen et al., 2019). The precursor gene is regulated by transcriptional targets of Serum Response Factor, Myocardin and NKX2–5, and they are required for smooth muscle development (Cordes et al., 2009). When taken together, it is possible that altered expression of these miRNAs played a potentially pathogenic role in the resulting *Dgcr8* phenotype that we observed. In the future, it will be necessary to examine multiple developmental stages to understand the changes and links between mRNA and miRNA genes. Nonetheless, because of the altered mRNA gene expression, along with pri-miRNA and mature miRNA expression levels may be first steps leading to the severe malformations observed later in mouse embryos.

Conclusions

Overall, we found that inactivation of *Dgcr8* in the aSHF resulted in a PTA with hypoplastic ventricles. The cardiac OFT and RV derive from the *Mef2c-AHF-Cre* lineage and these structures were severely affected. Early dysregulation of mRNA gene expression, increase in pri-miRNAs and decrease in miRNAs, in both the aSHF and OFT-RV, many important in cardiogenesis likely lead to the defects observed in *Dgcr8* cKO embryos.

Supplementary Material

Refer to Web version on PubMed Central for supplementary material.

Acknowledgements

We are grateful for the intellectual guidance on evaluating phenotypes on this project by Dr. Bin Zhou, Department of Genetics. We thank the Genomics Core at Einstein for performing Affymetrix gene expression arrays. We also want to thank the Histopathology Facility at Einstein.

Sources of funding

Our research is supported by National Institutes of Health [P01 HD070454 (BEM, DZ); R01 HL157157 (BEM, DZ), U54 HD090260 (BEM, DZ), and American Heart Association predoctoral fellowship [19PRE34380071 (LS)].

References

Ai D, Fu X, Wang J, Lu MF, Chen L, Baldini A, Klein WH, Martin JF, 2007. Canonical Wnt signaling functions in second heart field to promote right ventricular growth. Proc Natl Acad Sci U S A 104, 9319–9324. [PubMed: 17519332]

Botto LD, May K, Fernhoff PM, Correa A, Coleman K, Rasmussen SA, Merritt RK, O'Leary LA, Wong LY, Elixson EM, Mahle WT, Campbell RM, 2003. A population-based study of the 22q11.2 deletion: phenotype, incidence, and contribution to major birth defects in the population. Pediatrics 112, 101–107. [PubMed: 12837874]

Buckingham M, Meilhac S, Zaffran S, 2005. Building the mammalian heart from two sources of myocardial cells. Nat Rev Genet 6, 826–835. [PubMed: 16304598]

Carvalho BS, Irizarry RA, 2010. A framework for oligonucleotide microarray preprocessing. Bioinformatics 26, 2363–2367. [PubMed: 20688976]

Chapnik E, Sasson V, Blelloch R, Hornstein E, 2012. Dgcr8 controls neural crest cells survival in cardiovascular development. Developmental biology 362, 50–56. [PubMed: 22138056]

Chen X, Wang L, Huang R, Qiu H, Wang P, Wu D, Zhu Y, Ming J, Wang Y, Wang J, Na J, 2019. Dgcr8 deletion in the primitive heart uncovered novel microRNA regulating the balance of cardiac-vascular gene program. Protein Cell 10, 327–346. [PubMed: 30128894]

Chen Z, Wu J, Yang C, Fan P, Balazs L, Jiao Y, Lu M, Gu W, Li C, Pfeffer LM, Tigyi G, Yue J, 2012. DiGeorge syndrome critical region 8 (DGCR8) protein-mediated microRNA biogenesis is essential for vascular smooth muscle cell development in mice. J Biol Chem 287, 19018–19028. [PubMed: 22511778]

Cleynen I, Engchuan W, Hestand MS, Heung T, Holleman AM, Johnston HR, Monfeuga T, McDonald-McGinn DM, Gur RE, Morrow BE, Swillen A, Vorstman JAS, Bearden CE, Chow EWC, van den Bree M, Emanuel BS, Vermeesch JR, Warren ST, Owen MJ, Chopra P, Cutler DJ, Duncan R, Kotlar AV, Mulle JG, Voss AJ, Zwick ME, Diacou A, Golden A, Guo T, Lin JR, Wang T, Zhang Z, Zhao Y, Marshall C, Merico D, Jin A, Lilley B, Salmons HI, Tran O, Holmans P, Pardinas A, Walters JTR, Demaerel W, Boot E, Butcher NJ, Costain GA, Lowther C, Evers R, van Amelsvoort T, van Duin E, Vingerhoets C, Breckpot J, Devriendt K, Vergaelen E, Vogels A, Crowley TB, McGinn DE, Moss EM, Sharkus RJ, Unolt M, Zackai EH, Calkins ME, Gallagher RS, Gur RC, Tang SX, Fritsch R, Ornstein C, Repetto GM, Breetvelt E, Duijff SN, Fiksinski A, Moss H, Niarchou M, Murphy KC, Prasad SE, Daly EM, Gudbrandsen M, Murphy CM, Murphy DG, Buzzanca A, Fabio FD, Digilio MC, Pontillo M, Marino B, Vicari S, Coleman K, Cubells JF, Ousley OY, Carmel M, Gothelf D, Mekori-Domachevsky E, Michaelovsky E, Weinberger R, Weizman A, Kushan L, Jalbrzikowski M, Armando M, Eliez S, Sandini C, Schneider M, Bena FS, Antshel KM, Fremont W, Kates WR, Belzeaux R, Busa T, Philip N, Campbell LE, McCabe KL, Hooper SR, Schoch K, Shashi V, Simon TJ, Tassone F, Arango C, Fraguas D, Garcia-Minaur S, MoreyCanyelles J, Rosell J, Suner DH, Raventos-Simic J, International 22q, D.S.B., Behavior, C., Epstein MP, Williams NM, Bassett AS, 2021. Genetic contributors to risk of schizophrenia in the presence of a 22q11.2 deletion. Mol Psychiatry 26, 4496–4510. [PubMed: 32015465]

Cordes KR, Sheehy NT, White MP, Berry EC, Morton SU, Muth AN, Lee TH, Miano JM, Ivey KN, Srivastava D, 2009. miR-145 and miR-143 regulate smooth muscle cell fate and plasticity. Nature 460, 705–710. [PubMed: 19578358]

Cordes KR, Srivastava D, 2009. MicroRNA regulation of cardiovascular development. Circ Res 104, 724–732. [PubMed: 19325160]

De Bono C, Thellier C, Bertrand N, Sturny R, Jullian E, Cortes C, Stefanovic S, Zaffran S, Theveniau-Ruissy M, Kelly RG, 2018. T-box genes and retinoic acid signaling regulate the segregation of arterial and venous pole progenitor cells in the murine second heart field. Hum Mol Genet 27, 3747–3760. [PubMed: 30016433]

Doench JG, Sharp PA, 2004. Specificity of microRNA target selection in translational repression. Genes Dev 18, 504–511. [PubMed: 15014042]

Edelmann L, Pandita RK, Morrow BE, 1999a. Low-copy repeats mediate the common 3-Mb deletion in patients with velo-cardio-facial syndrome. Am J Hum Genet 64, 1076–1086. [PubMed: 10090893]

Edelmann L, Pandita RK, Spiteri E, Funke B, Goldberg R, Palanisamy N, Chaganti RS, Magenis E, Shprintzen RJ, Morrow BE, 1999b. A common molecular basis for rearrangement disorders on chromosome 22q11. Hum Mol Genet 8, 1157–1167. [PubMed: 10369860]

Erhardt S, Zheng M, Zhao X, Le TP, Findley TO, Wang J, 2021. The Cardiac Neural Crest Cells in Heart Development and Congenital Heart Defects. J Cardiovasc Dev Dis 8.

Goldmuntz E, 2020. 22q11.2 deletion syndrome and congenital heart disease. Am J Med Genet C Semin Med Genet 184, 64–72. [PubMed: 32049433]

Irizarry RA, Hobbs B, Collin F, Beazer-Barclay YD, Antonellis KJ, Scherf U, Speed TP, 2003. Exploration, normalization, and summaries of high density oligonucleotide array probe level data. Biostatistics 4, 249–264. [PubMed: 12925520]

Isakova A, Fehlmann T, Keller A, Quake SR, 2020. A mouse tissue atlas of small noncoding RNA. Proc Natl Acad Sci U S A 117, 25634–25645. [PubMed: 32978296]

John B, Enright AJ, Aravin A, Tuschl T, Sander C, Marks DS, 2004. Human MicroRNA targets. PLoS Biol 2, e363. [PubMed: 15502875]

Johnson WE, Li C, Rabinovic A, 2007. Adjusting batch effects in microarray expression data using empirical Bayes methods. Biostatistics 8, 118–127. [PubMed: 16632515]

Kelly RG, 2012. The second heart field. Curr Top Dev Biol 100, 33–65. [PubMed: 22449840]

Kelly RG, 2023. The heart field transcriptional landscape at single-cell resolution. Dev Cell 58, 257–266. [PubMed: 36809764]

Kelly RG, Buckingham ME, Moorman AF, 2014. Heart fields and cardiac morphogenesis. Cold Spring Harb Perspect Med 4.

Kirby ML, 1993. Cellular and molecular contributions of the cardiac neural crest to cardiovascular development. Trends Cardiovasc Med 3, 18–23. [PubMed: 21244966]

Lee EJ, Baek M, Gusev Y, Brackett DJ, Nuovo GJ, Schmittgen TD, 2008. Systematic evaluation of microRNA processing patterns in tissues, cell lines, and tumors. RNA 14, 35–42. [PubMed: 18025253]

Lewis BP, Burge CB, Bartel DP, 2005. Conserved seed pairing, often flanked by adenosines, indicates that thousands of human genes are microRNA targets. Cell 120, 15–20. [PubMed: 15652477]

Liu N, Bezprozvannaya S, Williams AH, Qi X, Richardson JA, Bassel-Duby R, Olson EN, 2008. microRNA-133a regulates cardiomyocyte proliferation and suppresses smooth muscle gene expression in the heart. Genes Dev 22, 3242–3254. [PubMed: 19015276]

McDonald-McGinn DM, Sullivan KE, Marino B, Philip N, Swillen A, Vorstman JA, Zackai EH, Emanuel BS, Vermeesch JR, Morrow BE, Scambler PJ, Bassett AS, 2015. 22q11.2 deletion syndrome. Nat Rev Dis Primers 1, 15071. [PubMed: 27189754]

Miller JA, Cai C, Langfelder P, Geschwind DH, Kurian SM, Salomon DR, Horvath S, 2011. Strategies for aggregating gene expression data: the collapseRows R function. BMC bioinformatics 12, 322. [PubMed: 21816037]

Nogami M, Miyamoto K, Hayakawa-Yano Y, Nakanishi A, Yano M, Okano H, 2021. DGCR8-dependent efficient pri-miRNA processing of human pri-miR-9–2. J Biol Chem 296, 100409. [PubMed: 33581109]

Nygaard V, Rodland EA, Hovig E, 2016. Methods that remove batch effects while retaining group differences may lead to exaggerated confidence in downstream analyses. Biostatistics 17, 29–39. [PubMed: 26272994]

Racedo SE, Hasten E, Lin M, Devakanmalai GS, Guo T, Ozbudak EM, Cai CL, Zheng D, Morrow BE, 2017. Reduced dosage of beta-catenin provides significant rescue of cardiac outflow tract anomalies in a Tbx1 conditional null mouse model of 22q11.2 deletion syndrome. PLoS Genet 13, e1006687. [PubMed: 28346476]

Rana MS, Theveniau-Ruissy M, De Bono C, Mesbah K, Francou A, Rammah M, Dominguez JN, Roux M, Laforest B, Anderson RH, Mohun T, Zaffran S, Christoffels VM, Kelly RG, 2014. Tbx1 coordinates addition of posterior second heart field progenitor cells to the arterial and venous poles of the heart. Circ Res 115, 790–799. [PubMed: 25190705]

Rao PK, Toyama Y, Chiang HR, Gupta S, Bauer M, Medvid R, Reinhardt F, Liao R, Krieger M, Jaenisch R, Lodish HF, Blelloch R, 2009. Loss of cardiac microRNA-mediated regulation leads to dilated cardiomyopathy and heart failure. Circ Res 105, 585–594. [PubMed: 19679836]

Ritchie ME, Phipson B, Wu D, Hu Y, Law CW, Shi W, Smyth GK, 2015. limma powers differential expression analyses for RNA-sequencing and microarray studies. Nucleic Acids Res 43, e47. [PubMed: 25605792]

Roth BM, Ishimaru D, Hennig M, 2013. The core microprocessor component DiGeorge syndrome critical region 8 (DGCR8) is a nonspecific RNA-binding protein. J Biol Chem 288, 26785–26799. [PubMed: 23893406]

Saga Y, Miyagawa-Tomita S, Takagi A, Kitajima S, Miyazaki J, Inoue T, 1999. MesP1 is expressed in the heart precursor cells and required for the formation of a single heart tube. Development 126, 3437–3447. [PubMed: 10393122]

Shaikh TH, Kurahashi H, Saitta SC, O'Hare AM, Hu P, Roe BA, Driscoll DA, McDonald-McGinn DM, Zackai EH, Budarf ML, Emanuel BS, 2000. Chromosome 22specific low copy repeats and the 22q11.2 deletion syndrome: genomic organization and deletion endpoint analysis. Hum Mol Genet 9, 489–501. [PubMed: 10699172]

Sousa VH, Miyoshi G, Hjerling-Leffler J, Karayannis T, Fishell G, 2009. Characterization of Nkx6–2-derived neocortical interneuron lineages. Cereb Cortex 19 Suppl 1, i1–10. [PubMed: 19363146]

Tyser RCV, Ibarra-Soria X, McDole K, Arcot Jayaram S, Godwin J, van den Brand TAH, Miranda AMA, Scialdone A, Keller PJ, Marioni JC, Srinivas S, 2021. Characterization of a common progenitor pool of the epicardium and myocardium. Science 371.

Unolt M, Versacci P, Anaclerio S, Lambiase C, Calcagni G, Trezzi M, Carotti A, Crowley TB, Zackai EH, Goldmuntz E, Gaynor JW, Digilio MC, McDonald-McGinn DM, Marino B, 2018. Congenital heart diseases and cardiovascular abnormalities in 22q11.2 deletion syndrome: From well-established knowledge to new frontiers. Am J Med Genet A 176, 2087–2098. [PubMed: 29663641]

Verzi MP, McCulley DJ, De Val S, Dodou E, Black BL, 2005. The right ventricle, outflow tract, and ventricular septum comprise a restricted expression domain within the secondary/anterior heart field. Developmental biology 287, 134–145. [PubMed: 16188249]

Vo NK, Dalton RP, Liu N, Olson EN, Goodman RH, 2010. Affinity purification of microRNA-133a with the cardiac transcription factor, Hand2. Proc Natl Acad Sci U S A 107, 19231–19236. [PubMed: 20974915]

Wang X, Chen D, Chen K, Jubran A, Ramirez A, Astrof S, 2017. Endothelium in the pharyngeal arches 3, 4 and 6 is derived from the second heart field. Developmental biology 421, 108–117. [PubMed: 27955943]

Wang Y, Medvid R, Melton C, Jaenisch R, Blelloch R, 2007. DGCR8 is essential for microRNA biogenesis and silencing of embryonic stem cell self-renewal. Nat Genet 39, 380–385. [PubMed: 17259983]

Warkala M, Chen D, Ramirez A, Jubran A, Schonning M, Wang X, Zhao H, Astrof S, 2021. Cell-Extracellular Matrix Interactions Play Multiple Essential Roles in Aortic Arch Development. Circ Res 128, e27–e44. [PubMed: 33249995]

Watanabe Y, Miyagawa-Tomita S, Vincent SD, Kelly RG, Moon AM, Buckingham ME, 2010. Role of mesodermal FGF8 and FGF10 overlaps in the development of the arterial pole of the heart and pharyngeal arch arteries. Circ Res 106, 495–503. [PubMed: 20035084]

Wystub K, Besser J, Bachmann A, Boettger T, Braun T, 2013. miR-1/133a clusters cooperatively specify the cardiomyogenic lineage by adjustment of myocardin levels during embryonic heart development. PLoS Genet 9, e1003793. [PubMed: 24068960]

Xie L, Hoffmann AD, Burnicka-Turek O, Friedland-Little JM, Zhang K, Moskowitz IP, 2012. Tbx5-hedgehog molecular networks are essential in the second heart field for atrial septation. Dev Cell 23, 280–291. [PubMed: 22898775]

Zare A, Salehpour A, Khoradmehr A, Bakhshalizadeh S, Najafzadeh V, Almasi-Turk S, Mahdipour M, Shirazi R, Tamadon A, 2023. Epigenetic Modification Factors and microRNAs Network Associated with Differentiation of Embryonic Stem Cells and Induced Pluripotent Stem Cells toward Cardiomyocytes: A Review. Life (Basel) 13.

Zhao Y, Ransom JF, Li A, Vedantham V, von Drehle M, Muth AN, Tsuchihashi T, McManus MT, Schwartz RJ, Srivastava D, 2007. Dysregulation of cardiogenesis, cardiac conduction, and cell cycle in mice lacking miRNA-1–2. Cell 129, 303–317. [PubMed: 17397913]

Zhao Y, Samal E, Srivastava D, 2005. Serum response factor regulates a muscle-specific microRNA that targets Hand2 during cardiogenesis. Nature 436, 214–220. [PubMed: 15951802]

Zhou L, Liu J, Xiang M, Olson P, Guzzetta A, Zhang K, Moskowitz IP, Xie L, 2017. Gata4 potentiates second heart field proliferation and Hedgehog signaling for cardiac septation. Proc Natl Acad Sci U S A 114, E1422–E1431. [PubMed: 28167794]

Highlights:

1. The *DGCR8* gene encodes a miRNA processing protein.
2. *DGCR8* is in the chromosome 22q11.2 region deleted in patients with 22q11.2DS.
3. Inactivation in the anterior second heart field results in severe heart defects.
4. Inactivation of *Dgcr8* in mice causes dysregulation of cardiac gene expression.
5. miRNAs important for cardiac development are decreased in expression.

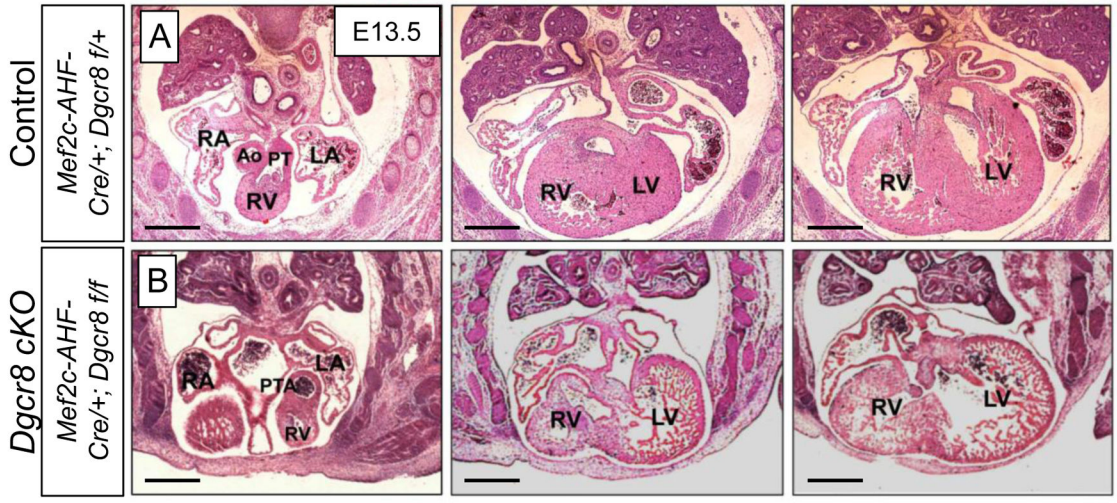

C Cardiac phenotypes at E13.5

Genotype	Total N	Stage	Normal (%)	PTA-VSD HyRV+LV
Control	22	E13.5	100	0
Dgcr8 cKO	27	E13.5	0	100

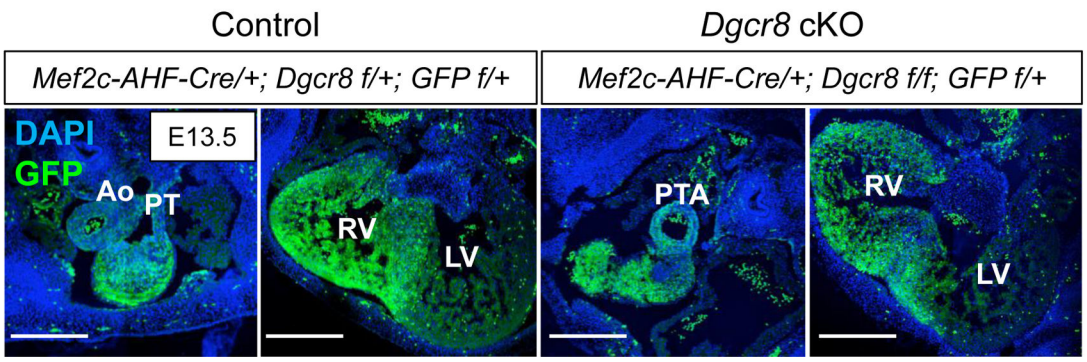

Figure 1. *Dgcr8* cKO mutants have a PTA and hypoplastic ventricles.

(A) Transverse H&E sections of control and **(B)** conditional mutant (bottom) hearts at E13.5 are shown. **(C)** Number of embryos with cardiac phenotypes. **(D)** Immunofluorescence staining for GFP on transverse paraffin sections to detect the derivatives of the aSHF cells in E13.5 in control versus *Dgcr8* cKO embryos. Ao: aorta, PT: pulmonary trunk, RA: right atrium, RV: right ventricle, LA: left atrium, LV: left ventricle, HyRV+LV: hypoplastic right and left ventricles. Scale bar in A, B and D: 0.5 mm.

A

Observed cardiac phenotype per stage

	Control		*Dgcr8* cKO	
Stage	Total N	Phenotype observed (%)	Total N	Phenotype observed (%)
E9.5	4	0	3	0
E10.5	6	0	8	0
E11.5	10	0	9	100 – HyRV
E12.5	10	0	12	100 – HyRV/PTA+VSD

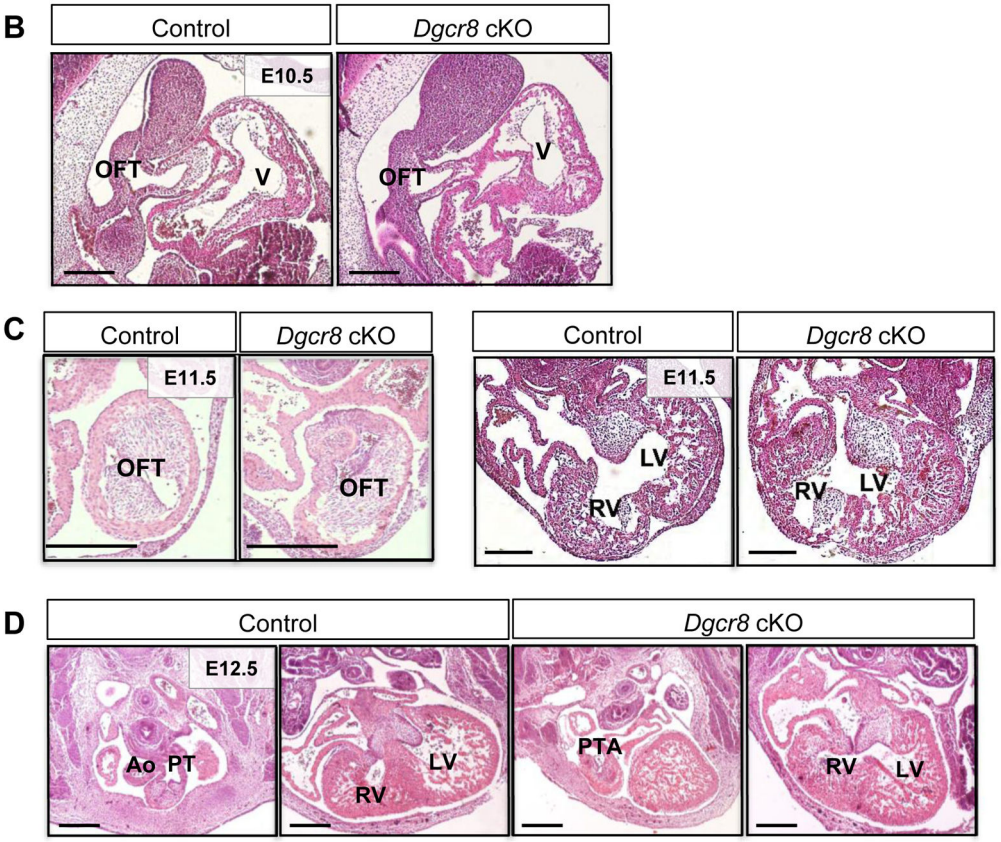

Figure 2. Malformations of the outflow tract and heart in *Dgcr8* cKO mutant embryos are apparent at E11.5 and E12.5.

(A) Table of phenotypes in control and *Dgcr8* cKO mutant embryos per stage. **(B)** H&E staining of sagittal sections showing no differences in morphology between control (upper image) and mutant (lower image) at E10.5. **(C)** H&E staining of a transverse section of the cardiac outflow tract (OFT) (left) and heart (right) at E11.5. *Dgcr8* embryos have a misalignment of OFT cushions. **(D)** H&E staining of transverse section of the aorta (Ao) and pulmonary trunk (PT) (left) and heart (right) at E12.5. HyRV: hypoplastic right ventricle; HyLV: hypoplastic left ventricle; PTA: persistent truncus arteriosus; RV: right ventricle, LV: left ventricle. Scale bar in B, C, D: 0.25 mm.

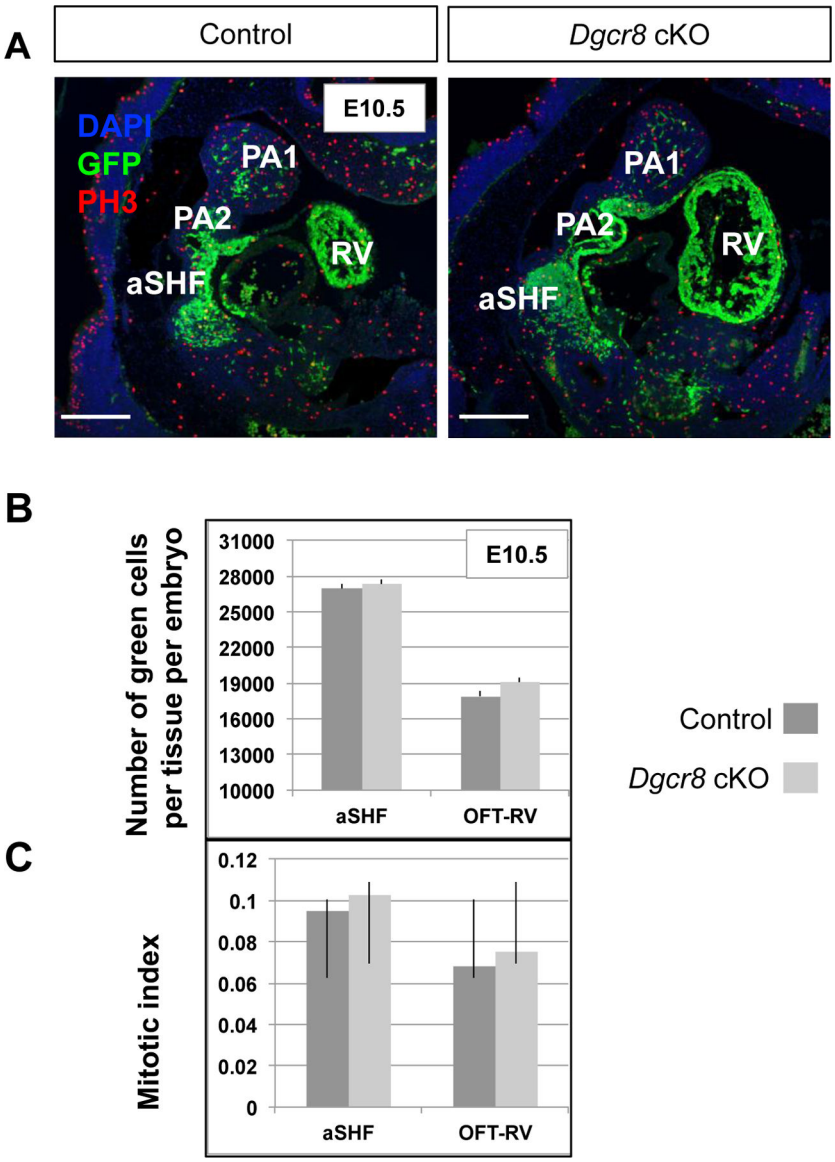

Figure 3. Normal cell number and mitotic index in *Dgcr8* cKO embryos at E10.5

(A) Sagittal section of control and *Dgcr8* cKO embryo in which the *Mef2c-AHF-Cre* lineage is marked by GFP (green) as compared to PH3 (red) and DAPI (blue) staining at E10.5. Scale bar in A: 0.3 mm. **(B)** Bar graph showing the number of green cells per tissue per embryo and **(C)** Bar graph for the mitotic index at E10.5. The mitotic index was calculated by taking the ratio of the proliferating cells in the aSHF to total counts of aSHF GFP positive cells. aSHF: anterior second heart field; PA1: pharyngeal arch 1; PA2: pharyngeal arch 2; OFT-RV: outflow tract and right ventricle. Statistical significance of the difference in gene expression was estimated of the four replicates using two-tailed t-test, FC is fold change, P values < 0.05. Error bars is standard deviation (SD).

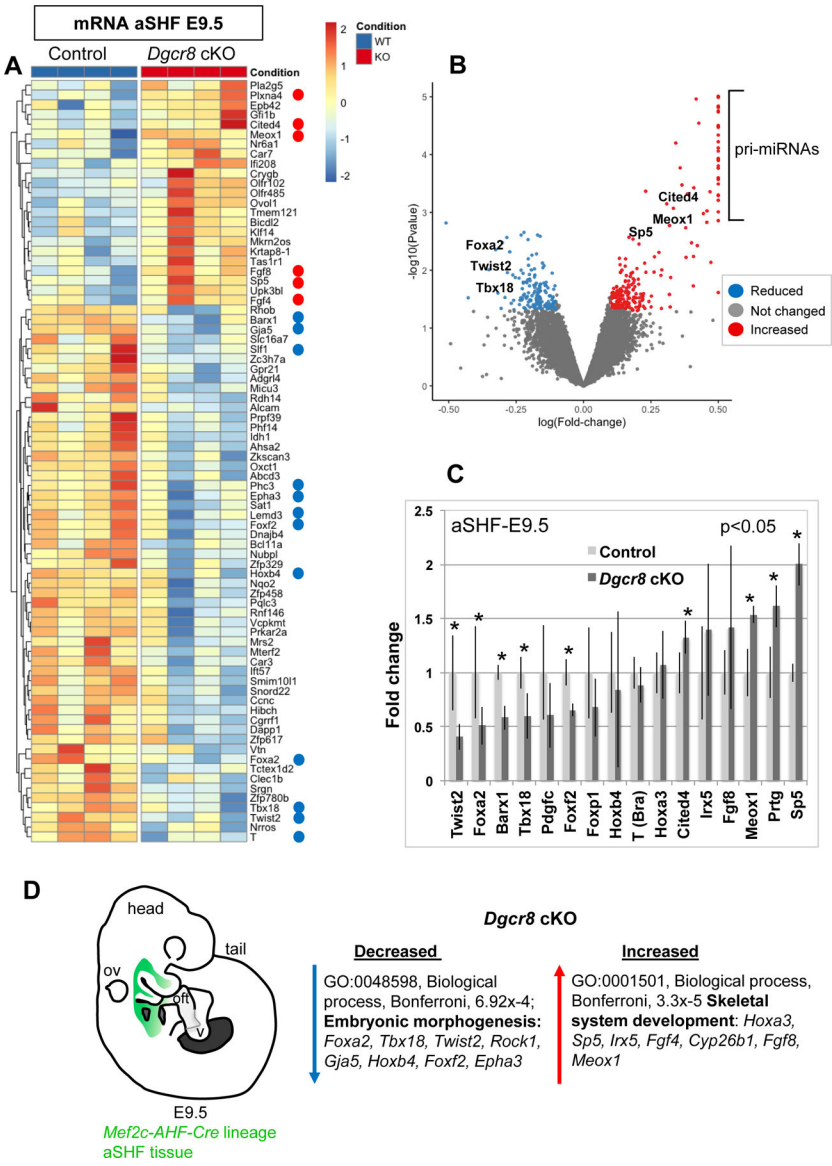

Figure 4. Gene expression analysis in the aSHF at E9.5.

(A) Heatmap showing gene expression changes for a selected set of differentially expressed genes in the microdissected aSHF of control and *Dgcr8* cKO embryos at E9.5. Plotted are differentially expressed genes ($p < 0.05$ and FC > 1.5). Circles next to genes indicate a subset of transcription factor and signaling genes selected for qRT-PCR and GO analysis (red is increased and blue is decreased in *Dgcr8* cKO embryos. **(B)** Volcano plot shows up-regulated and down-regulated genes ($p < 0.05$ and FC > 1.5). The expression changes for pri-miRNAs were truncated to fit in the plot and their actual fold changes can be found in Supplemental Table 10. **(C)** Validation of selected genes by qRT-PCR analysis in the aSHF of control and *Dgcr8* cKO embryos. Statistical significance of the difference in gene expression was estimated of the four replicates using two-tailed t-test, FC is fold change, P values < 0.05. Error bars is standard deviation (SD). **(D)** Illustration of the aSHF cells (green) that was dissected in an embryo at stage E9.5. GO of genes decreased or increased

in expression by hand curation of top transcription factors and signaling molecule genes are shown. Bonferroni corrected P values are indicated.

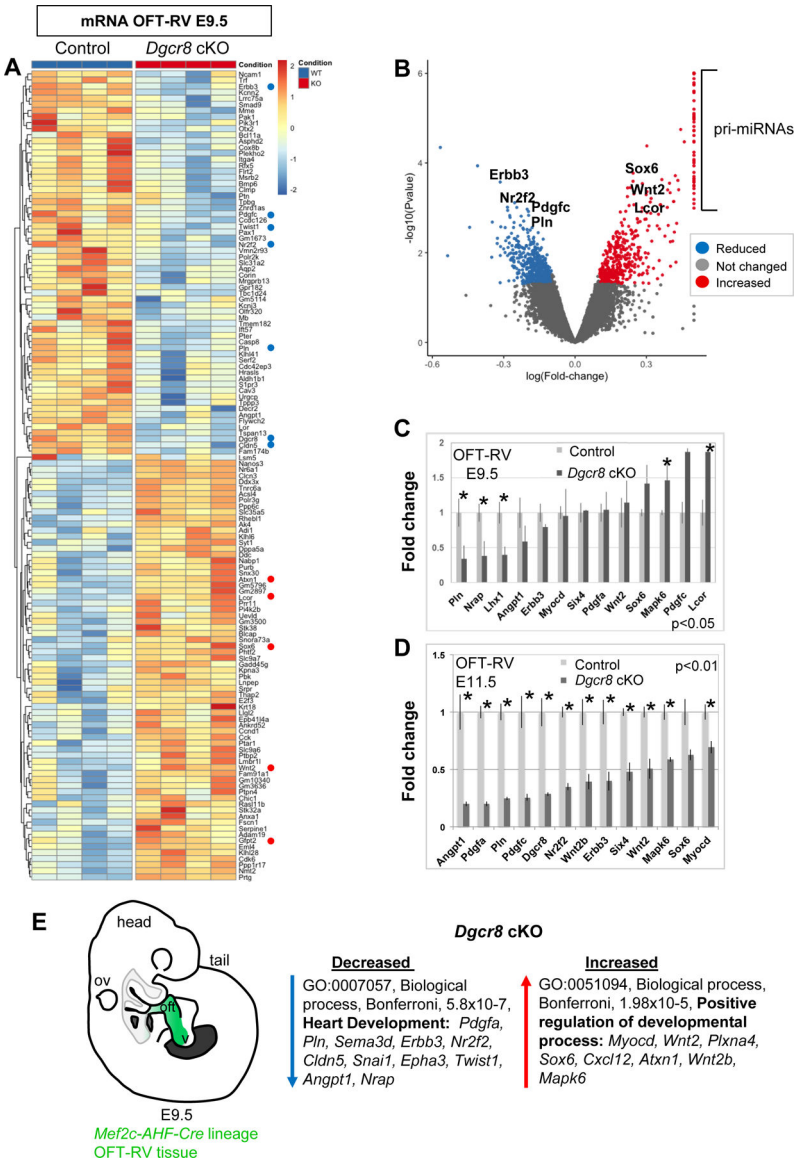

Figure 5. Gene expression analysis in the OFT-RV at E9.5 and E11.5.

(A) Heatmap showing gene expression changes for a selected set of DEGs in the microdissected OFT-RV of control and *Dgcr8* cKO at E9.5. Plotted are differentially expressed genes ($p < 0.05$ and FC > 1.5). Circles next to genes indicate a subset of transcription factor and signaling genes selected for qRT-PCR and GO analysis (red is increased and blue is decreased in *Dgcr8* cKO embryos. **(B)** Volcano plot shows up-regulated and down-regulated genes ($p < 0.05$ and FC > 1.5). The expression changes for pri-miRNAs are truncated to fit in the plot and their actual fold changes can be found in Supplemental Table 11. Validation of selected genes by qRT-PCR in control and *Dgcr8 LOF* embryos in the OFT-RV at E9.5 **(C)** and the RV at E11.5 **(D)**. Statistical significance of the difference in gene expression was estimated using two-tailed t-test, FC is fold change, P values < 0.05. Error bars is standard deviation (SD). **(E)** Illustration of the OFT-RV cells (green) that was dissected in an embryo at stage E9.5. GO of genes decreased or increased

in expression by hand curation of top transcription factors and signaling molecule genes are shown. Bonferroni corrected P values are indicated.

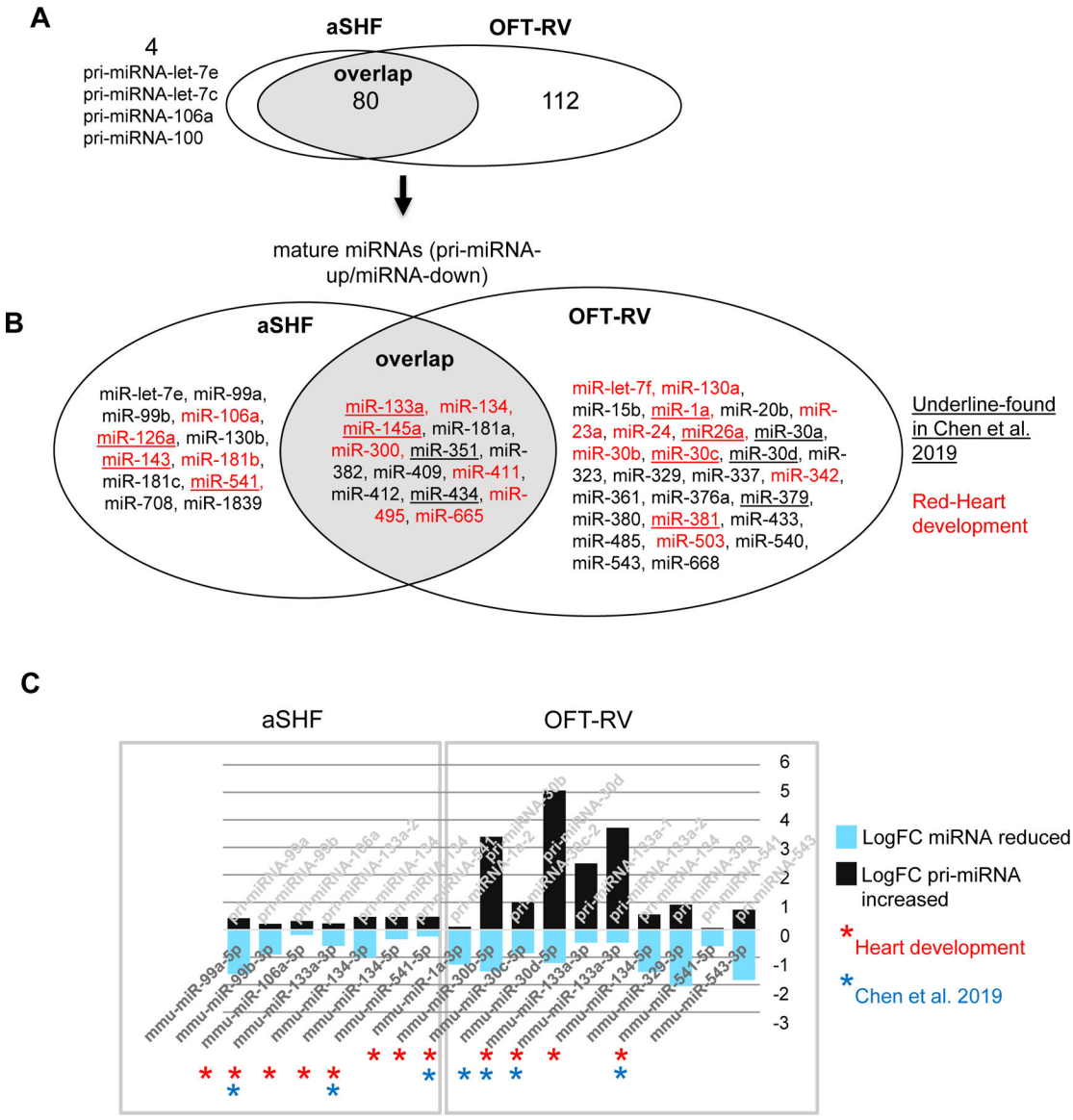

Figure 6. Comparison of pri-miRNAs and mature miRNAs relevant to cardiac development.

(A) Overlap of 80 pri-miRNA genes in the aSHF and OFT-RV that were increased in expression by inactivation of *Dgcr8* in the aSHF progenitor cells. Also shown are the number of pri-miRNA genes that are unique to the OFT-RV, as well as the list of four that are unique to the aSHF. **(B)** Overlap of mature miRNAs and unique miRNAs found in the aSHF and OFT-RV, of which their pri-miRNA genes were increased in expression, and the mature miRNAs were decreased in *Dgcr8* cKO tissues. Red color indicates genes relevant to heart development in Zare et al. (Zare et al., 2023) and underline are those miRNAs that were reduced in expression when *Dgcr8* was inactivated in the *Mesp1* lineage in Chen et al. (Chen et al., 2019). **(C)** Bar plot showing log fold-change (LogFC) of pri-miRNA genes (gray font; black color bars) and derivative miRNAs (black font, aqua bars) in the aSHF and OFT-RV. The miRNAs found that are relevant to heart development (Zare et al., 2023) are

shown with red stars and those reduced when *Dgcr8* was inactivated in the *Mesp1* lineage are shown with blue stars (Chen et al., 2019).